TÜBİTAK

Turkish Journal of Earth Sciences

http://journals.tubitak.gov.tr/earth/

Research Article

Turkish J Earth Sci
(2014) 23: 147-165

doi:10.3906/yer-1301-1

Chemistry of magmatic and alteration minerals in the Chahfiruzeh porphyry copper deposit, south Iran: implications for the evolution of the magmas and physicochemical conditions of the ore fluids

Morteza EINALI[1,2]*, Saeed ALIREZAEI[1], Federica ZACCARINI[3]

[1]Faculty of Earth Sciences, Shahid Beheshti University, Tehran, Iran

[2]Faculty of Sciences, Semnan University, Semnan, Iran

[3]Resource Mineralogy, Department of Applied Geosciences and Geophysics, University of Leoben, Leoben, Austria

Received: 02.01.2013 • **Accepted:** 05.11.2013 • **Published Online:** 18.01.2014 • **Printed:** 17.02.2014

Abstract: The Chahfiruzeh deposit is a newly discovered porphyry-style copper deposit in the southern part of the Cenozoic Urumieh-Dokhtar magmatic arc of Iran. Mineralization is associated with a Miocene quartz-diorite to quartz-monzodiorite porphyritic intrusion (Chahfiruzeh porphyry) intruded into older basaltic and andesitic lava flows and pyroclastic rocks. Alteration assemblages and alteration zoning, typical of porphyry copper deposits, are well developed. Mineralization occurs in quartz-sulfide stockworks and as sulfide disseminations in the porphyritic intrusion and the immediate wall rocks. Pyrite and chalcopyrite are the main hypogene sulfide minerals; bornite and molybdenite are rare. Representative magmatic and alteration minerals, including plagioclase, amphibole, biotite, sericite, and chlorite, are analyzed, and the data are used to constrain the crystallization conditions of the magmas and the nature and evolution of the hydrothermal fluids. The fluorine–chlorine fugacity in the magma during crystallization of the Chahfiruzeh porphyry, represented by log (fH_2O)/(fHF) – log (fH_2O)/(fHCl) and determined from the chemical composition of magmatic biotite, ranges between 5.23 and 6.80 and between 5.05 and 5.13, respectively. A comparison to several other intrusions associated with porphyry-style mineralization suggests that the Chahfiruzeh intrusion crystallized at relatively high fH_2O/fHCl ratios. The intercept value (F/Cl) of the magmatic biotite in the Chahfiruzeh porphyry ranges from 5.5 to 7.02. The calculated F/Cl intercept values for the biotite are consistent with those reported from many other porphyry copper systems. The secondary reequilibrated biotite in the intrusion is distinguished from the primary magmatic biotite by a slightly higher Mg component (X_{Mg} = 0.53–0.68 compared to 0.62–0.66). This can be explained by the consumption of Fe to form pyrite and chalcopyrite. Chlorite occurs as an alteration product replacing magmatic biotite and hornblende, as well as hydrothermal biotite. Chlorite geothermometry indicates a narrow range between 212 and 246 °C for the formation of chlorites from various alteration zones, implying that the whole system equilibrated with a common fluid at low temperatures.

Key words: Halogen chemistry, chlorite geothermometry, chlorine–fluorine fugacity, Chahfiruzeh porphyry, hornblende-plagioclase thermometer, Iran

1. Introduction

The Chahfiruzeh porphyry copper deposit is located in the southern section of the Cenozoic Urumieh-Dokhtar magmatic belt (Figure 1). Mineralization in Chahfiruzeh is associated with a Miocene quartz-monzodiorite to quartz-diorite porphyritic intrusion, intruded into older andesitic-basaltic lava flows and pyroclastic rocks (Mohammadzadeh, 2009). Hydrothermal alteration assemblages typical of porphyry copper deposits (PCDs) are well developed in Chahfiruzeh (Alirezaei and Mohammadzadeh, 2009). The ore reserve has been evaluated to be over 100 Mt (NICICO, 2008).

The chemical compositions of minerals in magmatic rocks provide invaluable information as to the origin, nature, and post-solidus modifications of the magmas, as well as the nature of the ore fluids associated with the magmas. In particular, the halogen (F, Cl) contents of biotite and hornblende can be used to investigate the characteristics and the evolution of the magmas and associated hydrothermal fluids (Imai, 2000; Selby and Nesbitt, 2000; Boomeri et al., 2009, 2010; Xianwu et al., 2009; Siahcheshm et al., 2012). The composition of hornblende has been used to estimate the crystallization temperature of magmas (e.g., Anderson and Smith, 1995), and the amount of ^{IV}Al substituting for Si in the tetrahedral site variations of chlorite has been indicated to be a function of temperature (Cathelineau and Nieva, 1985; Kranidiotis and McLean, 1987; Cathelineau, 1988; Battaglia, 1999).

* Correspondence: m_einali@sbu.ac.ir

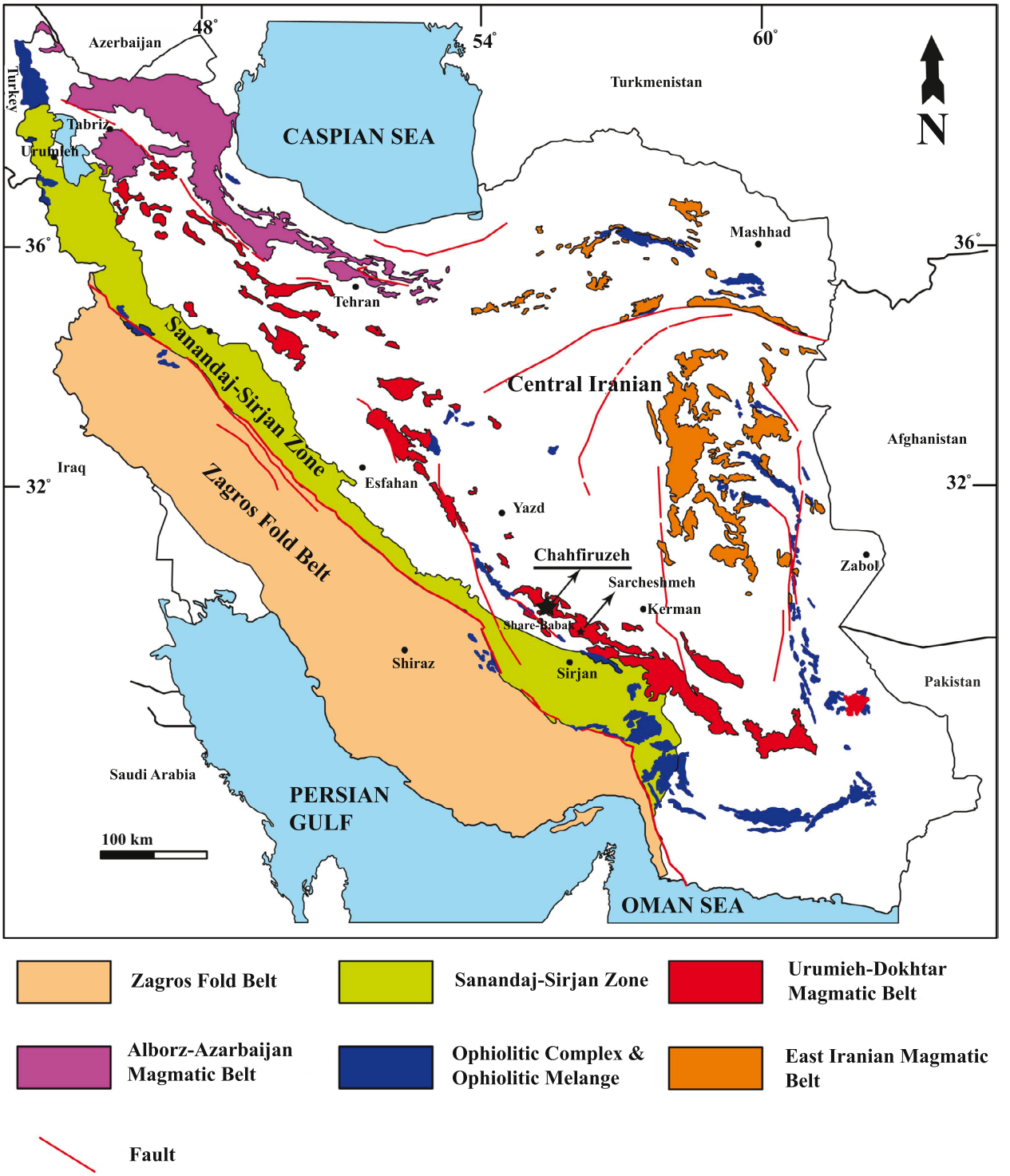

Figure 1. Simplified geological map of Iran, showing the main geological divisions [after Stöcklin (1968) and Aghanabati (1990)] and location of Chahfiruzeh and Sarcheshmeh porphyry systems.

In this study, we present data on the chemical compositions of the rock-forming minerals, plagioclase, biotite, and hornblende, as well as secondary hydrothermal biotite, sericite, chlorite, and sulfide minerals, and we discuss the nature and evolution of the magmas and hydrothermal fluids involved in alteration and mineralization in the Chahfiruzeh porphyry system.

2. Geological background and petrography

The Cenozoic was a time of active magmatism in Iran, represented by 3 major magmatic assemblages in West-Central (Urumieh-Dokhtar), North-Northwest (Alborz-Azarbaijan), and East Iran (Figure 1). The magmatism started in the late Cretaceous-Paleocene, peaked in the Eocene, and extended into the Miocene and Quaternary (e.g., Hassanzadeh, 1993; Verdel et al., 2011). The magmatism was associated with the formation of a wide range of ores, including an epithermal base and precious metal deposits, skarn-type base metal ores, and porphyry-type Cu-Mo-Au deposits (e.g., Richards et al., 2006; Alirezaei and Hasanpour, 2011; Ebrahimi et al., 2011; Kouhestani et al., 2011; Ashrafpour et al., 2012).

The majority of the known PCDs in Iran occur in the Urumieh-Dokhtar magmatic belt (UDMB) and its extension in Northwest Iran, the west end of the Alborz- Azarbaijan belt, known as the Arasbaran belt (Hasanpour, 2010; Alirezaei and Hasanpour, 2011) (Figure 1). The UDMB is dominated by calc-alkaline volcanic and intrusive rocks, and it is interpreted to be a continental magmatic arc, associated with subduction of the Neo-Tethyan oceanic crust beneath the central Iranian microcontinent and subsequent continental collision in the Miocene (e.g., Alavi, 1980, 1994; Berberian et al., 1982; Hassanzadeh, 1993; Agard et al., 2005; Shafiei et al., 2009; Verdel et al., 2011).

Most known PCDs in the UDMB occur in the southern section of the belt, also known as the Kerman Copper Belt (KCB). The Chahfiruzeh deposit is located in the central part of the KCB, about 95 km northwest of the world-class Sarcheshmeh PCD (Figure 1). The deposit is associated with a Miocene quartz-diorite to quartz-monzodiorite shallow pluton, here referred to as Chahfiruzeh porphyry, intruding into Eocene andesitic-basaltic lava flows and pyroclastic rocks (Figure 2). A crystallization age of 16.3 ± 0.1 Ma has been proposed for the intrusion based on zircon U-Pb dating (Kazemi Mehrnia, 2010). The intrusion is characterized by plagioclase, biotite, and lesser hornblende and quartz phenocrysts in a quartz-feldspar matrix (Figure 3a). Plagioclase occurs as euhedral to subhedral crystals and varies in size from 1 to 4 mm. Biotite occurs as euhedral crystals, 2–5 mm in diameter, and hornblende occurs as elongated euhedral crystals, 2–4 mm long.

The pluton and the enclosing volcanic rocks are intruded by a post-ore dioritic intrusion and associated dykes in the southern part of the deposit (Figure 2). The diorite consists of plagioclase, hornblende, and biotite phenocrysts in a feldspar- and quartz-rich groundmass (Figure 3b). Such late intrusions, particularly in the form of dykes, have been reported from many PCDs in the UDMB and elsewhere. Examples from the UDMB include biotite porphyry dykes in Sarcheshmeh (Waterman and Hamilton, 1975), andesitic dykes in Sungun (Hezarkhani, 2006), and diorite- to quartz-diorite dykes in Miduk (Taghipour et al., 2008). Hasanpour (2010) showed that the andesitic dykes in Sungun postdated the main stage of alteration-mineralization by less than 0.5 Ma.

The youngest magmatic activity in Chahfiruzeh is represented by a dacitic intrusion to the northeast of the deposit. The dacite contains numerous enclaves of the altered and mineralized Chahfiruzeh porphyry. It consists of plagioclase, quartz, hornblende, and biotite phenocrysts in a fine feldspar-quartz groundmass (Figure 3c).

Following a long period of uplift and erosion that led to the exposure of the deposit at the surface, the deposit was covered by a thick blanket of unconsolidated volcanic materials (lahar). Most lahar cover was subsequently eroded away, and the deposit was subjected to further weathering and erosion.

The Chahfiruzeh porphyry, the post-ore diorite, and the younger dacite all display calc-alkaline affinities and feature characteristics of intrusions emplaced in continental volcanic arc settings (Mohammadzadeh, 2009). This is consistent with data from many other Miocene intrusions associated with PCDs in the UDMB (e.g., Zarasvandi et al., 2005; Richards et al., 2006; Shafiei et al., 2009). The intrusive rocks in Chahfiruzeh display similar patterns in chondrite- and primitive mantle-normalized plots, implying a common magma source and evolution for the rocks (Alirezaei and Mohammadzadeh, 2009). They are distinguished by distinct enrichments in light rare earth elements relative to heavy rare earth elements; low Mg, Y, and Yb contents; and high Sr/Yb rations, features typical of adakitic or adakite-like magmas, as described by Defant and Drummond (1990), Richards and Kerrich (2007), Castillo (2012), and Richards et al. (2012).

2.1. Hydrothermal alteration-mineralization

Hydrothermal alteration has extensively affected the Chahfiruzeh porphyry and the host rocks. The alteration displays a broad zoning from a central, potassic assemblage, bordered by phyllic and propylitic assemblages outward. Silicic alteration and silica ledges locally occur at surface exposures. A supergene argillic alteration is superimposed on other alterations at surface and shallow depths. The paragenetic sequences of minerals from various alteration zones are presented in Figure 4.

Potassic alteration is characterized by abundant secondary biotite and subordinate K-spar, magnetite, and gypsum. Biotite occurs commonly as aggregates of fine (<100 μm), anhedral grains preferably replacing original magmatic hornblende and biotite, as well as a neoformed phase developed in the matrix and in veinlets. K-spar occurs in veinlets and as an alteration product replacing plagioclase.

Phyllic alteration is distinguished by the assemblage sericite, quartz ± chlorite, commonly associated with

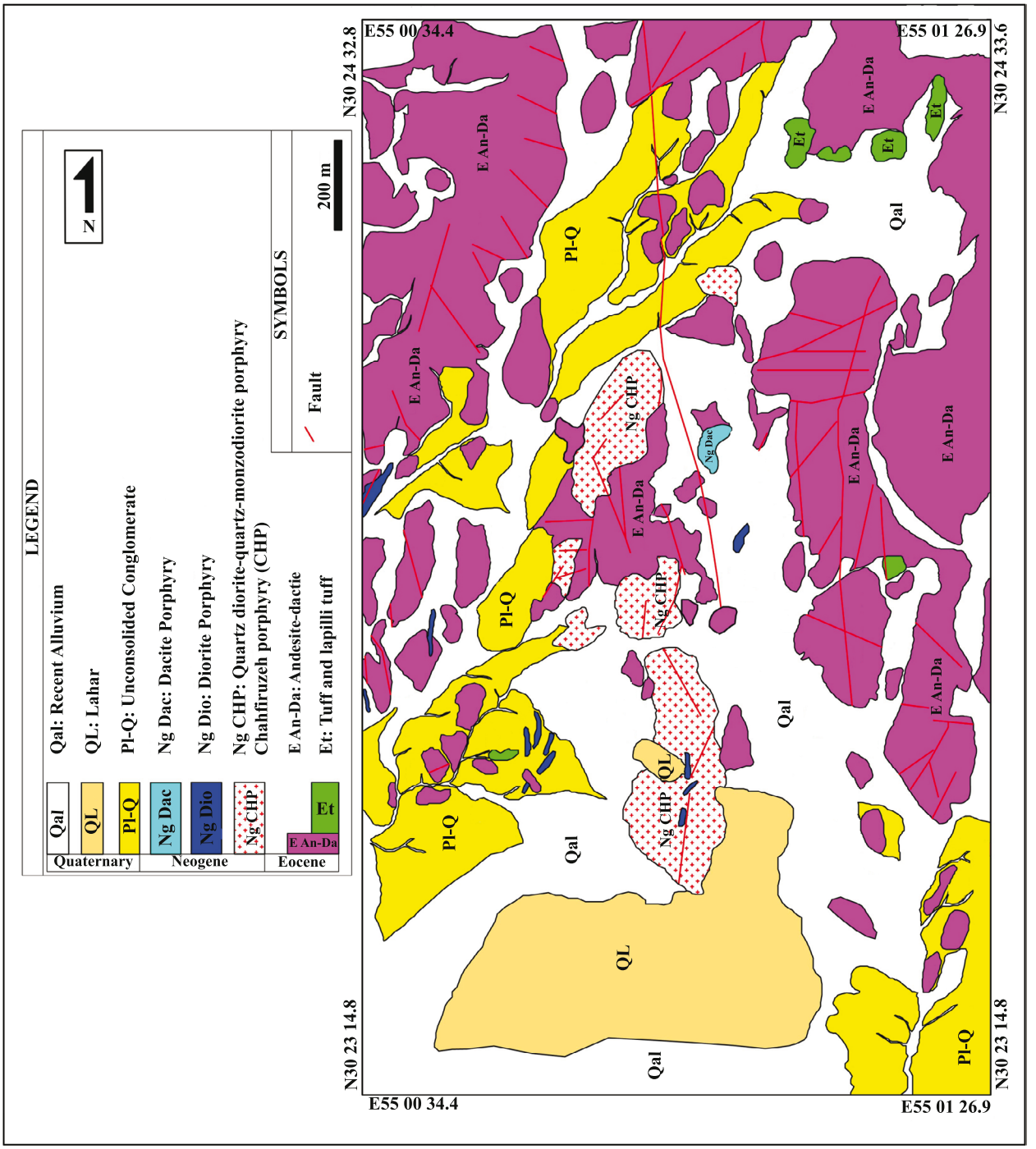

Figure 2. Geological map of the Chahfiruzeh porphyry system, modified after Mohammadzadeh (2009).

pyrite ± chalcopyrite. The alteration occurs across quartz-sulfide veinlets overprinting earlier potassic assemblages, as well as pervasive affecting large volumes of rocks. Propylitic alteration is developed in the volcanic host rocks with distance from the porphyritic pluton. The alteration is distinguished by variable carbonates (mostly calcite), epidote, and chlorite at the expense of plagioclase and mafic silicates. The late dioritic intrusion and associated dykes also display propylitic alteration, even where they cut rocks with potassic alteration.

Copper mineralization at Chahfiruzeh occurs as quartz-sulfide stockworks and sulfide disseminations associated with potassic and phyllic alteration assemblages. The hypogene sulfides include pyrite, chalcopyrite, and rare bornite and molybdenite. An oxide zone dominated by malachite is well

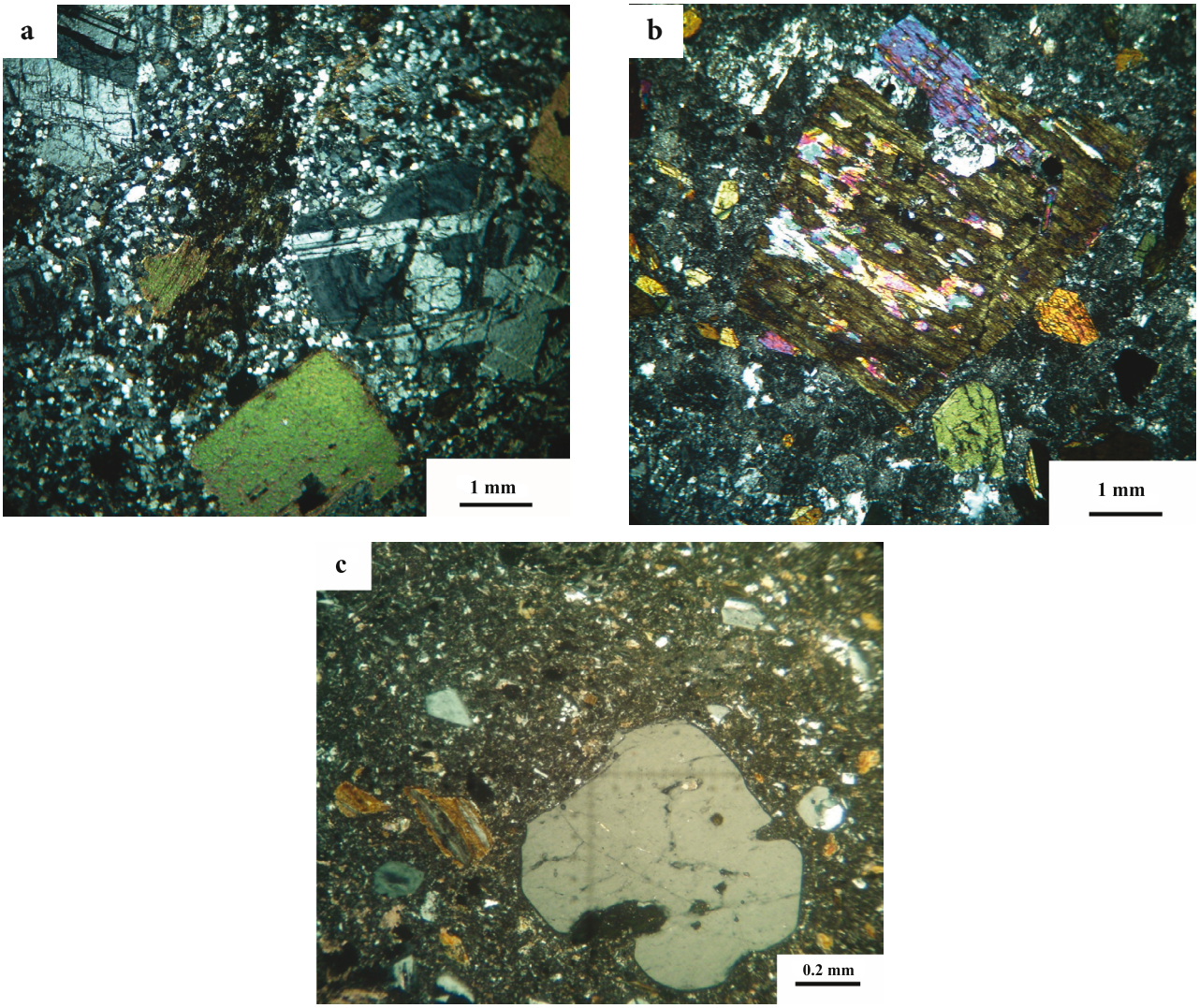

Figure 3. Images showing the mineralogy and textures of intrusive rocks from Chahfiruzeh. a) Microphotograph showing plagioclase and biotite phenocrysts in a quartz-rich matrix. Hornblende phenocryst (elongated crystal in center) is completely replaced by secondary hydrothermal biotite. b) Microphotograph showing replacement of biotite phenocryst by chlorite; several hornblende crystals can be distinguished. The diorite is typified by plagioclase, hornblende, and subordinate biotite phenocrysts in a quartz-feldspar-hornblende matrix. c) Microphotograph showing resorbed quartz and biotite phenocrysts in a quartz-rich matrix. The sample is from the dacite porphyry.

developed in the southern part of the deposit, where it was mined for several years in the 1990s. A supergene enriched blanket, up to 40 m thick, occurs in the deposit. The late diorite is locally rich in pyrite; however, the copper assay rarely exceeds 0.1%.

3. Materials and methods

Primary magmatic and secondary alteration minerals from various rocks collected from drill cores (Table 1) were analyzed with a Superprobe Jeol JXA 8200 instrument at the Eugen F. Stumpfl Laboratory of Leoben University, Austria. Back-scattered electron images were obtained using the same instrument. The analyses were conducted in WDS mode with 15 kV accelerating voltage and 10 nA beam current. The beam diameter was about 1 μm. Analyses for Mg, Al, Ti, Si, Ca, Na, K, F, Cl, Mn, and Fe were carried out using the Kα lines and were calibrated on natural adularia, atacamite, rhodonite, titanite, fluorite, labradorite, wollastonite, and olivine. The counting times for peaks and backgrounds (upper and lower) were 20 and 10 s, respectively. The following diffracting crystals were used: TAP for Na, Mg, and Al; PETJ for Ti and Cl; PETH for Si, Ca, and K; and LIFH for Fe and Mn. The detection limits, calculated for each element by the instrument software, are (in wt.%): 0.01 for

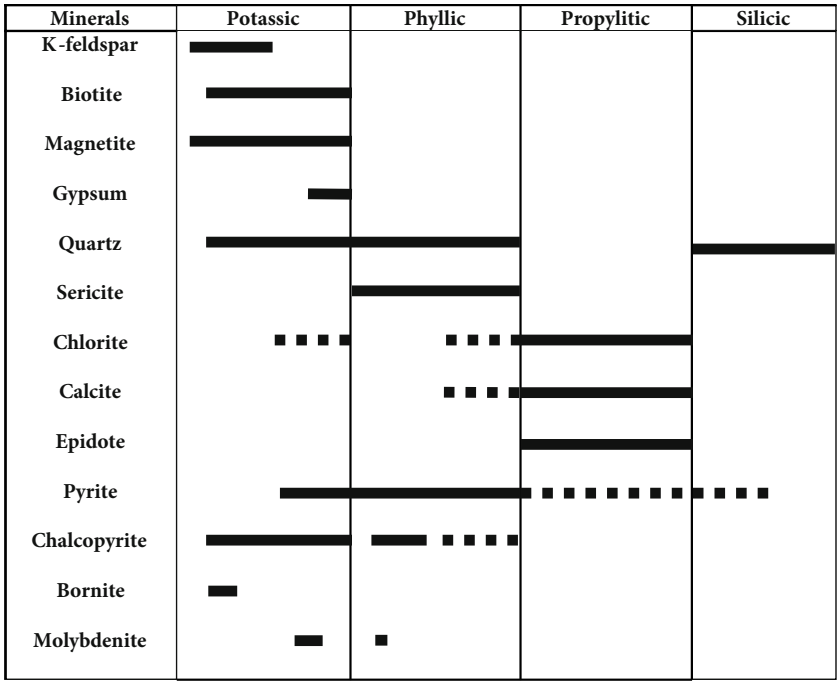

Figure 4. Paragenetic sequences for various alteration-mineralization zones in the Chahfiruzeh porphyry system.

Mg, Al, Si, Ca, K, and Cl; 0.02 for Na; 0.03 for Ti, Fe, and Mn; and 0.25 for F.

The sulfides were analyzed by electron microprobe in the WDS mode, at 20 kV accelerating voltage and 10 nA beam current, using a beam diameter of about 1 μm or less. The counting time for peaks and backgrounds were 20 and 10 s, respectively. The Kα lines were used for S, As, Fe, Cu, Co, Ni, and Zn; Lα for Mo; and Mα for Pb. The reference materials were synthetic NiS, natural chalcopyrite, galena, molybdenite, skutterudite, sphalerite, and niccolite for Ni, Fe, Cu, Pb, Mo, Co, Zn, S, and As. The following diffracting crystals were selected: PETJ for S; PETH for Mo and Pb; LIFH for Fe, Cu, Co, Ni, and Zn; and TAP for As.

4. Mineral chemistry

The chemical compositions of the primary magmatic minerals, and the minerals developed in the course of hydrothermal alteration and mineralization, were determined to investigate the physicochemical conditions of the magma and the fluids involved in alteration and mineralization in the Chahfiruzeh deposit. To save space, here we present only the chemical compositions of the primary magmatic minerals; data for other minerals will be provided upon request.

4.1. Amphibole

Amphibole is a common Fe-Mg mineral in the Chahfiruzeh porphyry; however, it is variably replaced by secondary biotite and chlorite. The post-ore dioritic intrusion and associated dykes have been indicated to be cogenetic with the Chahfiruzeh porphyry and emplaced at the same crustal levels (Alirezaei and Mohammadzadeh, 2009; Mohammadzadeh, 2009). As a proxy, fresh amphibole phenocrysts from a diorite dyke were analyzed.

Table 1. Characteristics of samples selected for electron microprobe analyses; abbreviations after Whitney and Evans (2010).

Sample code	Rock type	Location	Alteration	Mineral assemblage		Mineral analyzed
Borehole/depth				Major	Minor	
CHF06/413	CHP	Central part	Pervasive phyllic	Ser, Qz, Opaque	Chl, Pl	Pl, Ser, Chl
CHF31/578.30	CHP	Central part	Moderate potassic	Pl, Bt, Qz, Kfs	Chl, Ttn, Opq	Pl, Bt, Qz, Kfs, Chl
CHF35/416.5	Andesite	Central part	Strong potassic	Pl, Bt	Chl, Qz, Opq	Pl, Bt, Chl
CHF30/550.40	Diorite	Central part	Moderate propylitic	Pl, Hbl, Kfs	Qz, Ep, Chl, Ttn, Opq	Pl, Hbl, Kfs, Ep, Chl

Table 2. Chemical composition of primary hornblende (rim) cogenetic with plagioclase (rim) within post-ore diorite.

Sample (CHF30-550.40)			
Analysis	AN45	AN46	AN56
SiO2	44.856	46.360	43.873
TiO2	1.221	1.154	1.442
Al2O3	7.590	6.827	8.466
FeO	15.367	14.651	15.787
MnO	0.447	0.391	0.451
MgO	12.518	13.360	12.060
CaO	11.313	11.356	11.326
Na2O	1.292	1.121	1.360
K2O	0.898	0.764	1.089
F	0.233	0.118	0.000
Cl	0.020	0.011	0.020
Total	95.760	96.110	95.870
Structural formula calculation is based on 23 oxygens, using 15-NK calculation method.			
Si^{IV}	6.815	6.958	6.673
Al^{IV}	1.185	1.042	1.327
Al^{VI}	0.173	0.165	0.189
Fe^{+3}	0.178	0.143	0.196
Ti	0.140	0.130	0.165
Mg	2.835	2.989	2.734
Fe^{+2}	1.775	1.696	1.812
Mn	0.058	0.05	0.058
Ca	1.842	1.826	1.846
Na	0.381	0.326	0.401
K	0.174	0.146	0.211
Σ Cations	15.560	15.470	15.610
X_{Mg}	0.61	0.64	0.60
X_{Fe+2}	0.39	0.36	0.40
Ab	64.4	57.6	68.3
An	29.3	38.6	26.2
P* (kbar)	1.26	1.38	1.90
T** (°C)	740.3	796.7	739.4

*Calculation after Anderson and Smith (1995).
**Calculation after Holland and Blundy (1994).

Amphibole composition was calculated to an atoms per formula unit (a.p.f.u.) of 23 oxygen and normalized to total cations (Na + K) = 15, following Hawthorne (1981). Ferric iron was calculated according to the method described by Robinson et al. (1981). The amphibole phenocrysts vary in composition from magnesio-hornblende to edenite. The phenocrysts are rich in the Mg component (X_{Mg} = 0.58–0.71 and X_{Fe+2} = 0.29–0.42), and in this respect they compare with amphiboles reported from many intrusive rocks associated with porphyry Cu mineralization worldwide (e.g., Imai, 2000; Idrus et al., 2007).

A hornblende–plagioclase thermometer was calibrated according to the method of Holland and Blundy (1994) using 2 exchange reactions, including 1) edenite + 4 quartz = albite + tremolite; and 2) edenite + albite = anorthite + richterite. The first exchange reaction applies to quartz-bearing assemblages and is adopted in the present study.

Amphibole from the post-ore diorite is characterized by 0.30–0.65 a.p.f.u. Na, 0.14–0.42 a.p.f.u. Al^{VI}, 6.08–7.05 a.p.f.u. Si, and X_{Mg} = 0.58–0.71. The coexisting plagioclase has a composition varying from $Ab_{57.6}$ to $Ab_{68.3}$. The composition of the amphibole meets the criteria of Holland and Blundy (1994) and can be used in hornblende–plagioclase thermometric calculations. The calculations suggest a mean temperature of 758.8 ± 18 °C for the emplacement of the post-ore diorite and, by analogy, the main porphyritic intrusion (Table 2).

An Al-in-hornblende barometer potentially offers a basis for estimation of the crystallization pressure for granitic rocks (Anderson and Smith, 1995). The temperatures obtained by the hornblende–plagioclase thermometer were used to determine the pressure at emplacement. Using the equation of Anderson and Smith (1995), our calculations suggest that the post-ore diorite was emplaced at approximately 1.51 ± 0.6 kbar, consistent with a depth of approximately 6 km (Table 2).

4.2. Feldspar

Plagioclase is a major constituent of intrusive rocks in Chahfiruzeh. Plagioclase phenocrysts were analyzed from the Chahfiruzeh porphyry, a post-ore diorite dyke, and the host andesitic volcanic rocks.

The composition of the primary plagioclase phenocrysts preserved in the phyllic and potassic alteration zones in the Chahfiruzeh porphyry ranges from $Ab_{96.4}$ to $Ab_{98.6}$ and $Ab_{61.2}$ to $Ab_{86.8}$, respectively. The high Ab component in plagioclase from the phyllic alteration zone can be attributed to post-solidus, hydrothermal reactions involving introduction of Na. Sodium metasomatism and development of albite at the expense of calcic plagioclases during phyllic alteration has been reported from several PCDs (e.g., Hezarkhani, 2006; Idrus et al., 2007).

The composition of plagioclase phenocrysts in the post-ore diorite ranges from $Ab_{57.6}$ to $Ab_{84.3}$, which is broadly consistent with that in the Chahfiruzeh porphyry with potassic alteration. The composition of plagioclase in the host andesite displays a narrow range ($Ab_{46.4}$ to $Ab_{47.9}$) and is distinctly more calcic than those in the Chahfiruzeh porphyry and the post-ore diorite.

Table 3. Chemical composition of primary magmatic biotite from the Chahfiruzeh porphyry.

	CHF31-578.30						
	AN19	AN49	AN55	AN83	AN87	AN92	AN93
SiO_2	37.324	37.083	37.117	36.908	37.095	37.062	37.227
TiO_2	3.045	3.150	2.984	2.499	3.710	4.302	4.089
Al_2O_3	13.625	14.321	14.224	13.627	13.988	13.831	13.82
FeO	14.984	15.406	15.616	15.466	15.408	15.545	15.847
MnO	0.049	0.060	0.052	0.070	0.041	0.076	0.112
MgO	15.027	15.654	15.147	16.892	14.917	14.772	14.703
CaO	0.000	0.039	0.067	0.100	0.000	0.000	0.000
Na_2O	0.171	0.212	0.163	0.147	0.203	0.290	0.283
K_2O	9.600	9.322	9.471	7.471	9.721	9.703	9.606
F	1.492	1.225	0.821	0.629	0.502	0.046	0.685
Cl	0.041	0.040	0.045	0.040	0.048	0.046	0.040
H2O (calc.)	3.620	3.810	3.970	4.040	4.130	4.360	4.060
Total	98.340	99.800	99.320	97.620	99.540	100.000	100.170
	Cations based on 22 anions (afu):						
Si	5.163	5.056	5.090	5.096	5.079	5.056	5.075
Al^{IV}	2.220	2.299	2.297	2.216	2.256	2.222	2.219
Tetrahedral site	7.383	7.355	7.387	7.312	7.335	7.278	7.294
Ti	0.317	0.323	0.308	0.260	0.382	0.441	0.419
Fe_2	1.733	1.757	1.791	1.786	1.764	1.773	1.807
Mn	0.006	0.007	0.006	0.008	0.005	0.009	0.013
Mg	3.099	3.182	3.097	3.477	3.045	3.004	2.988
Ca	0.000	0.006	0.010	0.015	0.000	0.000	0.000
Octahedral site	5.155	5.275	5.212	5.546	5.196	5.227	5.227
Na	0.046	0.056	0.043	0.039	0.054	0.077	0.075
K	1.694	1.621	1.657	1.316	1.698	1.689	1.671
Interlayer	1.740	1.677	1.700	1.355	1.752	1.766	1.746
Anions (afu):							
F	1.305	1.056	0.712	0.549	0.435	0.040	0.591
Cl	0.019	0.018	0.021	0.019	0.022	0.021	0.018
OH (calc.)	3.338	3.463	3.633	3.716	3.771	3.970	3.695
X_{Mg}	0.64	0.64	0.63	0.66	0.63	0.63	0.62
X_{Fe}	0.36	0.36	0.37	0.34	0.37	0.37	0.38
X_{phl}	0.60	0.60	0.59	0.63	0.59	0.57	0.57
X_{Sid}	0.14	0.16	0.17	0.14	0.16	0.15	0.15
X_{An}	0.22	0.20	0.20	0.20	0.21	0.22	0.23
Log (X_{Mg}/X_{Fe})	0.25	0.25	0.23	0.29	0.23	0.23	0.21
Log (X_F/X_{OH})	–0.41	–0.52	–0.71	–0.83	–0.94	–2.00	–0.80
Log (X_{Cl}/X_{OH})	–2.24	–2.28	–2.24	–2.29	–2.23	–2.28	–2.31
Log (X_F/X_{Cl})	1.84	1.77	1.53	1.46	1.30	0.28	1.52
IV(F)	1.501	1.604	1.784	1.947	2.016	3.076	1.864
IV(Cl)	–4.000	–3.961	–3.988	–3.992	–3.992	–3.949	–3.894
IV(F/Cl)	5.502	5.565	5.772	5.939	6.008	7.025	5.758
Log (fH2O)/(fHF)	5.23	5.34	5.51	5.68	5.74	6.80	5.59
Log (fH2O)/(fHCl)	5.07	5.11	5.06	5.13	5.05	5.09	5.12
Log (fHF)/(fHCl)	–1.16	–1.23	–1.45	–1.59	–1.68	–2.70	–1.44

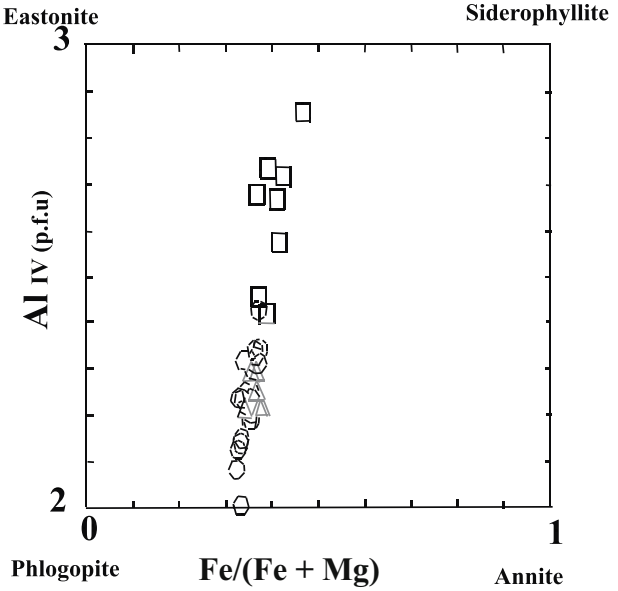

Figure 5. Plots of the magmatic and hydrothermal biotites on the Al^{IV} versus Fe/(Fe + Mg) quadrilateral diagram. Symbols: primary (triangle) and secondary (circle) biotite from CHP; secondary biotite (square) from andesite.

4.3. Biotite

Three types of biotites were analyzed: 1) primary magmatic biotite from the Chahfiruzeh porphyry; 2) secondary biotite replacing primary biotite and hornblende in the Chahfiruzeh porphyry; and 3) neoformed biotite occurring in matrix in the host andesite.

Primary magmatic biotite is locally well preserved in the Chahfiruzeh porphyry, particularly in rocks with potassic alteration. The biotite is characterized by a high and consistent Mg component (X_{Mg} ratio between 0.62 and 0.66), but relatively low Al^{IV} content (2.21 to 2.29 apfu) (Table 3). The biotite plots near the phlogopite corner (Figure 5).

Plots of the magmatic biotites on the ternary MgO-FeO_{tot}-Al_2O_3 discrimination diagram, proposed by Abdel-Rahman (1994), suggest a calc-alkaline, orogenic-related setting for the Chahfiruzeh porphyry and associated mineralization (Figure 6). This is consistent with interpretations based on the whole rock chemistry, as mentioned earlier. The Mg-rich character of the primary biotite in the Chahfiruzeh porphyry is consistent with data from many other PCDs reported in the literature (Jacobs and Parry, 1976, 1979; Beane and Titley, 1981; Mason, 1987; Selby and Nesbitt, 2000).

The secondary, reequilibrated biotite also plots close to the phlogopite corner (Figure 5); however, it is distinguished from the primary biotite by a slightly higher Mg component (X_{Mg} ranging from 0.53 to 0.68). The rather similar composition of the primary and secondary reequilibrated biotites suggests that the former was in equilibrium with the fluids responsible for the potassic alteration. The slightly higher MgO and lower FeO values in the reequilibrated biotite could be explained by the removal of iron to form pyrite and chalcopyrite. The neoformed biotite from the andesitic host rock is characterized by relatively high Al^{IV} values (Figure 5).

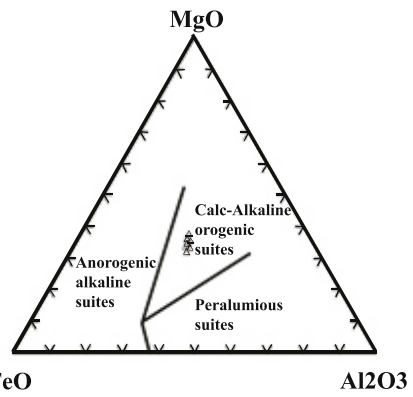

Figure 6. Plots of magmatic biotites from Chahfiruzeh porphyry on the Ternary FeO-MgO-Al_2O_3 diagram of Abdel-Rahman (1994). Total iron is presented as FeO.

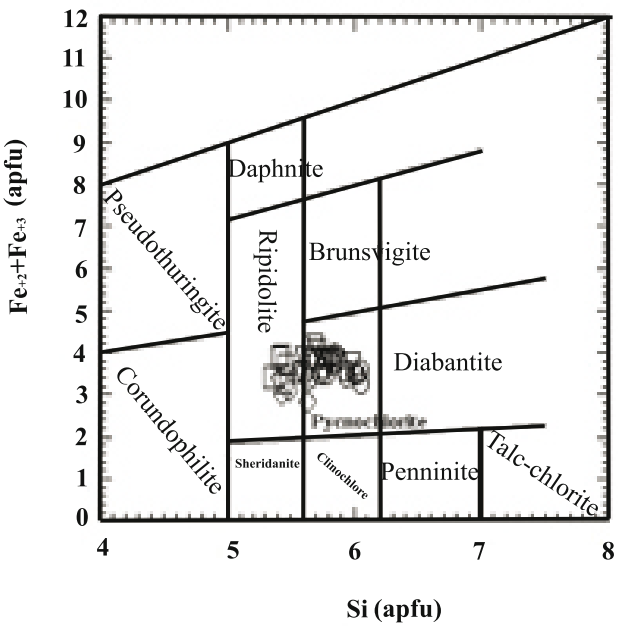

Figure 7. Plots of chlorites from various alteration assemblages in Chahfiruzeh, on the Si (apfu) vs. Fe^{+2} +Fe^{+3} (apfu) diagram of Deer et al. (1972). Symbols: Potassic alteration in the CHP (circle), potassic alteration in the andesite (diamond), phyllic alteration in the CHP (square), propylitic alteration of diorite (triangle).

The secondary neoformed biotite from the andesite with potassic alteration is characterized by higher Al_2O_3, FeO, and K_2O and lower F, Na_2O, and TiO_2 contents compared to the primary and reequilibrated biotites from the Chahfiruzeh porphyry. The difference in composition may be attributed to changes in fluid composition with time and with distance from the source of the fluid, and to original variations in the mineralogy and geochemistry of the 2 rocks.

4.4. Sericite

Sericite was analyzed from a specimen with pervasive phyllic alteration in the Chahfiruzeh porphyry (Table 1, Appendix 1). The sericite displays a relatively wide range in Na_2O and K_2O contents (0.12–0.47 and 7.75–11.81 wt.%, respectively) and in Al/Si atomic ratio (0.33–0.46). This could be due to changes in the fluid composition as well as the chemistry of the original mineral being replaced. Variations in K_2O are positively correlated with MgO contents.

4.5. Chlorite

Chlorite occurs as: 1) overprint on earlier secondary biotite in rocks with dominant potassic alteration (Type 1); 2) associated with sericite in phyllic alteration (Type 2); 3) replacing magmatic biotite and hornblende in propylitic alteration (Type 3). Chemical formula were calculated from electron microprobe analyses on the basis of 14 oxygens per formula unit (Appendix 2). The chlorites range in composition from pynochlorite to ripidolite based on the classification of Deer et al. (1972) (Figure 7). The chlorite from phyllic alteration has higher Al_2O_3 content (18.23–21.12 wt.%) compared to chlorite from potassic alteration (16.3–19.83 wt.%). Chlorite from potassic alteration in the host andesite displays the highest Al_2O_3 and lowest FeO contents. Chlorite from propylitic alteration in the post-ore diorite is relatively enriched in MnO and depleted in MgO and TiO_2. The chlorite is also distinguished by higher X_{Fe} (0.4 to 0.44) compared to those from potassic and phyllic alterations in the Chahfiruzeh porphyry.

Chlorite geothermometry was used, following the method described by Kranidiotis and MacLean (1987), to constrain the formation temperatures of chlorites from various alteration zones. The temperatures vary in a narrow range between 212 to 246 °C, and no significant differences can be distinguished among the various chlorites. The low temperatures of formation calculated for chlorite is consistent with data from fluid inclusion studies, where an assemblage with homogenization temperatures in the range 240–260 °C has been distinguished (Einali, unpublished data).

4.6. Sulfide minerals

Chalcopyrite is the main hypogene copper mineral at Chahfiruzeh; bornite occurs locally as a minor phase. Chalcopyrite is common in both phyllic and potassic alteration zones; bornite, however, occurs only in the potassic zone. The minerals were analyzed for variations in Mo, As, Ni, Co, Zn, and Pb, besides the main constituents, S, Fe, and Cu. Both minerals were found to be close to their ideal compositions ($CuFeS_2$ and Cu_5FeS_4, respectively).

Chalcopyrite accommodates higher contents of Mo (0.45–0.65 wt.%, mean 0.57 wt.%) relative to bornite (0.36–0.51 wt.%, mean 0.42 wt.%). Chalcopyrite from the potassic zone was found to be enriched in Zn (<0.01–0.19 wt.%) and Pb (<0.01–0.09 wt.%), compared to that from the phyllic zone (<0.01–0.14 wt.% and <0.01–0.06 wt.%, respectively).

Bornite carries higher contents of Pb (<0.01–0.22 wt.%) compared to chalcopyrite from both potassic and phyllic zones (<0.01–0.05 wt.% and <0.01–0.15 wt.%, respectively). Bornite and chalcopyrite from the potassic zone contain similar contents of Zn (0.01–0.1 and <0.01–0.18 wt.%, respectively); chalcopyrite from the phyllic zone, however, is depleted in Zn (<0.01–0.09 wt.%).

5. Halogen chemistry

Magmatic biotite composition is useful in the calculation of the fluorine and chlorine fugacities in magma during crystallization, which are represented by log (fHF/fH$_2$O) and log (fHCl/fH$_2$O), respectively (e.g., Ague and Brimhall, 1988; Zhu and Sverjensky, 1992). Halogen fugacity can be computed using the equations of Munoz (1992), which are based on the revised coefficients for the halogen–hydroxyl exchange (Zhu and Sverjensky, 1992):

$$\text{Log } (f\,H_2O)/(f\,HF)^{fluid} = 1000 / T\,(2.37 + 1.1\,(X_{Mg})^{bio}) + 0.43 - \log\,(X_F/X_{OH})^{bio},$$

$$\text{Log } (f\,H_2O)/(f\,HCl)^{fluid} = 1000 / T\,(1.15 + 0.55\,(X_{Mg})^{bio}) + 0.68 - \log\,(X_{Cl}/X_{OH})^{bio},$$

$$\text{Log } (f\,HF)/(f\,HCl)^{fluid} = -1000 / T\,(1.22 + 1.65\,(X_{Mg})^{bio}) + 0.25 + \log\,(X_F/X_{Cl})^{bio}.$$

The crystallization temperature for the Chahfiruzeh porphyry is assumed to be around 760 °C by analogy with the temperature calculated for the diorite, as well as temperatures reported in the literature for crystallization of similar intrusions (e.g., Idrus et al., 2007).

Using the equations of Munoz (1992), the log values for fH$_2$O/fHF, fH$_2$O/fHCl, and fHF/fHCl in the Chahfiruzeh porphyry magma fall in the ranges of 5.23–6.80, 5.05–5.13, and –1.16 to –2.70, respectively (Table 3). A comparison to several other intrusions associated with porphyry-style mineralization suggests that the Chahfiruzeh porphyry crystallized at higher fH$_2$O/fHCl ratios (Figures 8 a and 8b). The fHF/fHCl ratios can be compared to those of the other intrusions (Figure 8b); however, the fH$_2$O/fHF ratios plot near the lower end of the values reported for other intrusions (Figure 8a).

X_{Mg}, X_{sid}, and X_{ann} (siderophyllite and annite mole fractions, respectively) for biotite from the Chahfiruzeh porphyry were used to calculate the halogen intercept values, IV(F), IV(Cl), and IV(F/Cl) (Table 3). X_{sid} and

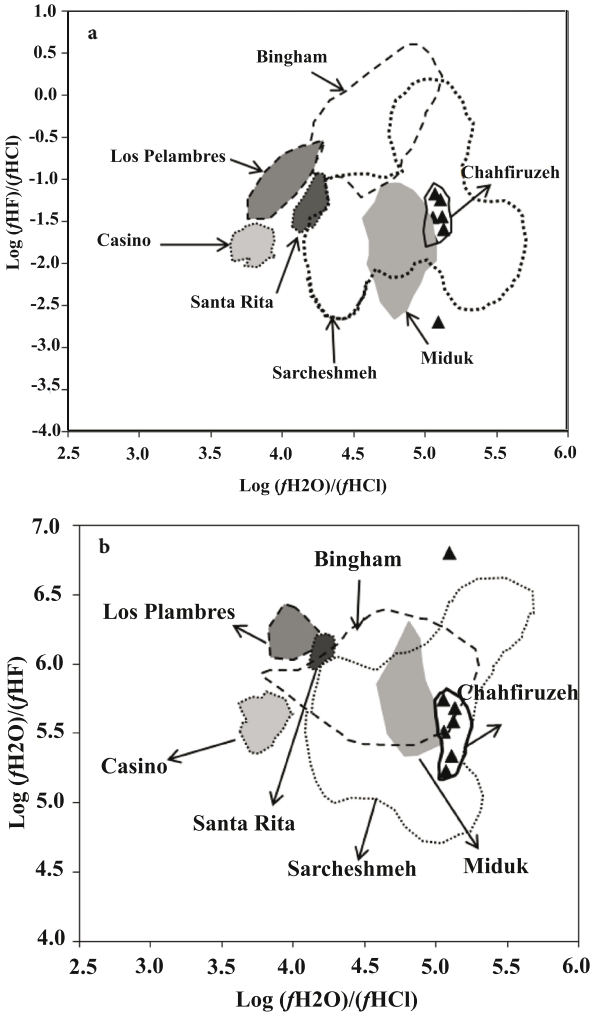

Figure 8. The calculated halogen fugacity ratios of magma in equilibrium with biotite for Chahfiruzeh porphyry; ratios for several other intrusions associated with porphyry-style mineralization are shown for comparison. a) log (*f*HF/*f*HCl) versus log (fH_2O/*f*HCl); b) log (fH_2O/*f*HF) versus log (fH_2O/*f*HCl). Data for other intrusions: Bingham (Lanier et al., 1978; Parry et al., 1978; Bowman et al., 1987), Casino (Selby and Nesbitt, 2000), Miduk (Boomeri et al., 2009), Sarcheshmeh (Boomeri et al., 2010), Los Pelambres (Taylor, 1983), and Santa Rita (Jacobs and Parry, 1979).

X_{ann} in biotite were obtained from the following equations (after Gunow et al., 1980):

$X_{sid} = (3 - Si/Al)\ 1.75 \times (1 - X_{phl})$,

$X_{ann} = 1 - (X_{phl} - X_{sid})$.

The intercept values (IVs) were introduced to define single numerical values that express the relative degrees of F or Cl enrichments in mica, and the values are temperature- independent (Munoz, 1984). The IV(F) and IV(Cl) for biotite were defined by Munoz (1984) using the following equations:

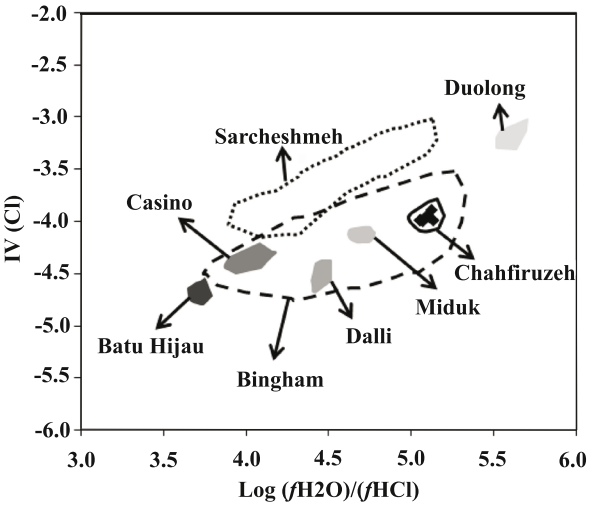

Figure 9. Plots of the log (fH_2O/*f*HCl) versus IV(Cl) values for Chahfiruzeh magmatic biotites; values for several other intrusions associated with porphyry-style deposits are shown for comparison. Data for other intrusions: Bingham (Lanier et al., 1978; Parry et al., 1978; Bowman et al., 1987), Casino (Selby and Nesbitt, 2000), Dalli (Ayati et al., 2008), Miduk (Boomeri et al., 2009), Sarcheshmeh (Boomeri et al., 2010), Duolong (Li et al., 2011), and Batu Hijau (Idrus et al., 2007).

$IV(F)_{biotite} = 1.52\ X_{Mg} + 0.42\ X_{An} + 0.20\ X_{sid} - \log (X_F / X_{OH})$,

$IV(Cl)_{biotite} = -5.01 - 1.93\ X_{Mg} - \log (X_{Cl} / X_{OH})$.

Magmatic biotites from the Chahfiruzeh porphyry display a narrow range (–3.89 to –4.00) in IV(Cl) values (Table 3). A broad correlation exists between fH_2O/*f*HCl ratios and IV(Cl) values when various deposits are plotted (Figure 9), with Chahfiruzeh being distinguished by relatively high log fH_2O/*f*HCl ratios and IV(Cl) values.

The $IV(F)_{biotite}$ values for the Chahfiruzeh porphyry vary between 1.5 and 3.07 (Table 3) and compare with those established by Munoz (1984) for shallow intrusions associated with porphyry-style Cu deposits. The $IV(F/Cl)_{biotite}$ values are directly related to the *f*(HCl)/*f*(HF) ratios, because they are independent of the temperature of equilibrium and the OH^- content of the mica (Munoz, 1984). The $IV(F/Cl)_{biotite}$ values for the Chahfiruzeh porphyry vary between 5.5 and 7.02 (Table 3). The values are similar to those established by Munoz (1984) for biotite in several PCDs. The lower IV(F/Cl) values correspond to higher F/Cl ratios.

Variations in the Mg/Fe and F/OH ratios in magmatic biotite can be used to investigate contamination in the igneous rocks (Ague and Brimhall, 1988). The term "contamination" has been used by the authors, in a broad sense, to refer to interactions of mafic I-type magmas derived from upper mantle or subducted slabs with

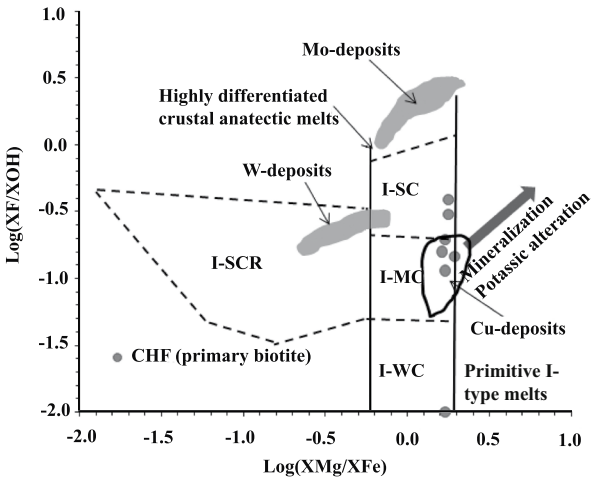

Figure 10. Plots of the Chahfiruzeh magmatic biotite in log (X_{Mg}/X_{Fe}) versus log (X_F/X_{OH}) discrimination diagram of Brimhall and Crerar (1987) for granitic intrusions: I-MC: I-type moderately contaminated; I-SC: I-type strongly contaminated; ISCR, I-type strongly contaminated and reduced; I-WC: I-type weakly contaminated.

continental crustal source components by such processes as partial melting, magma mixing, and assimilation. I-type granitoids containing biotite with log (X_{Mg}/X_{Fe}) > –0.21 have been divided by Brimhall and Crerar (1987) into 3 subgroups based upon increasing F/OH ratios (Figure 10). The 3 subgroups of the I-type granitoids are characterized by high oxidation states. The granitoids containing biotite with log (X_{Mg}/X_{Fe}) < –0.21 have been classified as strongly contaminated and reduced (I-SCR type).

Plots of the Chahfiruzeh magmatic biotites on the log (X_{Mg}/X_{Fe}) versus log (X_F/X_{OH}) discrimination diagram of Brimhall and Crerar (1987) indicate that the intrusion crystallized from a moderately to strongly crustal-contaminated, I-type granitic magma (Figure 10).

6. Discussion

Al-hornblende thermobarometry suggests that the post-ore diorite was emplaced at 758 ± 18 °C under a lithostatic pressure of 1.50 kbar. Considering the close spatial and temporal association, the same conditions would apply to the Chahfiruzeh porphyritic intrusion.

The higher albite component in the magmatic plagioclase phenocrysts preserved in the phyllic alteration zone compared to that in the potassic zone ($Ab_{96.4}$ to $Ab_{98.6}$ and $Ab_{61.2}$ to $Ab_{86.8}$, respectively) in the Chahfiruzeh porphyry can be attributed to post-solidus, hydrothermal reactions. An original magmatic effect on the composition of plagioclase is ruled out, since crystal fractionation is expected to result in the formation of increasingly Na-rich plagioclases inward.

Lead and zinc chloride complexes are more stable in hydrothermal fluids at acidic pH conditions characteristic of phyllic alteration in a porphyry environment (e.g., John, 2010). This has resulted in the precipitation of chalcopyrite with lower Zn and Pb contents in the phyllic alteration zone compared to that associated with potassic alteration assemblages that commonly form under less acidic conditions.

Unlike in silicates, limited data are available on the chemistry of sulfides in porphyry systems. Pasava et al. (2010) and Hanley et al. (2010) investigated the distribution of platinum-group elements in pyrite from the Kalmakyr porphyry deposit in Uzbekistan. In a recent study, Reich et al. (2013) investigated the distribution of precious metals, metalloids, and heavy metals in pyrite from the Dexing porphyry deposit in China. Our data indicate that the chemistry of sulfide minerals is mainly controlled by the characteristics of the fluids at any time in the course of the evolution of the hydrothermal system.

Biotite is the main alteration product in the potassic zone and occurs as replacing primary magmatic hornblende and biotite (reequilibrated biotite), as well as a newly formed phase in the matrix (neoformed biotite). The 2 types of biotites display narrow ranges in Fe/(Fe + Mg) ratios, but variable Al^{IV} contents, in the Chahfiruzeh porphyry. The neoformed biotites from potassic alteration in the host andesite are distinguished by higher Al^{IV} in the tetrahedral layer.

Both magmatic and alteration biotites are Mg-rich, with X_{Mg} ranging from 0.53 to 0.68 corresponding to a phlogopite mole fraction (X_{Phl}) of 0.50 to 0.64. Enrichment in Mg in phlogopite- annite solid solution, as in the Chahfiruzeh hydrothermal biotites, can be attributed to relatively high oxygen and/or sulfur fugacities (Wones and Eugster, 1965; Wones, 1972; Tso et al., 1979) and consumption of iron to form magnetite, pyrite, and/or chalcopyrite. The neoformed and reequilibrated biotites in the Chahfiruzeh intrusion are characterized by higher Al_2O_3, FeO, and K_2O and lower F, Na_2O, and TiO_2 contents compared to the primary magmatic biotite. Chlorite occurs as an alteration product associated with sericite in the phyllic zone, as well as an overprint on secondary biotite in the potassic zone, and as replacing magmatic hornblende and biotite in the propylitic zone. Chlorites from various alteration zones in the Chahfiruzeh porphyry system formed at similarly low temperatures (212 to 246 °C), implying that the whole system equilibrated with a common fluid at low temperatures.

The halogen (fluorine–chlorine) fugacity for the Chahfiruzeh porphyry parent magma, as calculated from the composition of magmatic biotites, ranges between 5.23 and 6.80 and between 5.05 and 5.13, respectively. The fugacity ranges are comparable to those calculated for mineralizing intrusions in the Sarcheshmeh and Miduk PCDs, Iran (Boomeri et al., 2009, 2010). Compared to other porphyry systems, magmatic biotite from Chahfiruzeh shows a narrow range in log(fH_2O/fHF) values. The lower

log (*f*HF/*f*HCl) values for Chahfiruzeh is consistent with the Cl-rich nature of the hydrothermal fluids.

Magmatic biotites from the Chahfiruzeh porphyry display a narrow range, between –3.89 to –4.00, in IV(Cl) values, similar to that reported for magmatic biotite from the Miduk PCD (Boomeri et al., 2009) but slightly lower than that in the Sarcheshmeh PCD (Boomeri et al., 2010). The IV(F) values vary between 1.50 and 3.07, similar to those reported from the Sarcheshmeh and Miduk PCDs (Boomeri et al., 2009, 2010).The IV(F/Cl) values range from 5.50 to 7.02. The biotites show a similar range of IV (F/Cl) values corresponding to a Cl-rich system rather than an F-rich system. The composition of magmatic biotite from the Chahfiruzeh porphyry is consistent with crystallization from a moderately to strongly contaminated I-type granitic magma.

Acknowledgments

This contribution is part of the first author's PhD thesis project, with laboratory studies carried out at the Department of Applied Geosciences and Geophysics, University of Leoben, Austria. Appreciation is extended to Professor Ronald Bakker for generously providing access to the laboratory facilities and to Helmut Müllenhaus for preparing thin-polished samples.

References

Abdel-Rahman AM (1994). Nature of biotites from alkaline, calc-alkaline, and peraluminous magmas. J Petrol 35: 525–541.

Agard P, Omrani J, Jolivet L, Mouthereau F (2005). Convergence history across Zagros (Iran): Constraints from collisional and earlier deformation. Int J Earth Sci 94: 401–419.

Aghanabati A (1990). Magmatic Rocks of Iran. Geological Survey of Iran; Scale 1:2,500,000, 1 sheet. Tehran, Iran: Geological Survey of Iran.

Ague JJ, Brimhall GH (1988). Magmatic arc asymmetry and distribution of anomalous plutonic belts in the batholiths of California: effects of assimilation, cratonal thickness and depth of crystallization. Geol Soc Am Bull 100: 912–927.

Alavi M (1980). Tectonostratigraphic evolution of Zagros sides of Iran. Geology 8: 144–149.

Alavi M (1994). Tectonic of the Zagros orogenic belt of Iran: new data and interpretations. Tectonophysics 229: 211–238.

Alirezaei S, Hasanpour S (2011). An overview of porphyry copper deposits in Iran. In: The 1st World Copper Congress, Iran; Proceedings with Abstracts, pp. 49–62.

Alirezaei S, Mohammadzadeh Z (2009). Hydrothermal alteration-mineralization at Chahfiroozeh porphyry copper deposit, Kerman province, southern Iran. In: Geological Association of Canada-Mineralogical Association of Canada-American Geophysical Union Joint Assembly, Toronto, Abstract GA71A-15.

Anderson JL, Smith DR (1995). The effect of temperature and oxygen fugacity on Al-in-hornblende barometry. Am Mineral 80: 549–559.

Ashrafpour E, Ansdell KM, Alirezaei S (2012). Hydrothermal fluid evolution and ore genesis in the Arghash epithermal gold prospect, northeastern Iran. J Asian Earth Sci 51: 30–44.

Ayati F, Yavuz F, Noghreyan M, Haroni HA, Yavuz R (2008). Chemical characteristics and composition of hydrothermal biotite from the Dalli porphyry copper prospect, Arak, central province of Iran. Miner Petrol 94: 107–122.

Battaglia S (1999). Applying X-ray geothermometer diffraction to a chlorite. Clays Clay Miner 47: 54–63.

Beane RE, Titley SR (1981). Porphyry copper deposits. Part II. Hydrothermal alteration and mineralization. Econ Geol 75th Anniversary Volume: 235–263.

Berberian F, Muir ID, Pankhurst RJ, Berberian M (1982). Late Cretaceous and early Miocene Andean type plutonic activity in northern Makran and central Iran. J Geol Soci London 139: 605–614.

Boomeri M, Nakashima K, Lentz DR (2009). The Miduk porphyry Cu deposit, Kerman, Iran: a geochemical analysis of the potassic zone including halogen element systematics related to Cu mineralization processes. J Geochem Explor 103: 17–29.

Boomeri M, Nakashima K, Lentz DR (2010). The Sarcheshmeh porphyry copper deposit, Kerman, Iran: A mineralogical analysis of the igneous rocks and alteration zones including halogen element systematic related to Cu mineralization processes. Ore Geol Rev 38: 367–381.

Bowman JR, Parry WT, Kropp WP, Kruer SA (1987). Chemical and isotopic evolution of hydrothermal solutions at Bingham, Utah. Econ Geol 82: 395–428.

Castillo PR (2012). Adakite petrogenesis. Lithos 134: 304–316.

Cathelineau M (1988). Cation site occupancy in chlorites and illites as a function of temperature. Clay Miner 23: 471–485.

Cathelineau M, Nieva D (1985). A chlorite solid solution geothermometer. The Los Azufres (Mexico) geothermal system. Contr Miner Petrol 91: 235–244.

Deer WA, Howie, RA, Zussman J (1972). An Introduction to the Rock-Forming Minerals. 2nd ed. Essex, UK: Pearson.

Defant MJ, Drummond MS (1990). Derivation of some modern arc magmas by melting of the subducted lithosphere in a volcanic arc. Geology 21: 547–550.

Ebrahimi S, Alirezaei S, Pan Y (2011). Geological setting, alteration, and fluid inclusion characteristics of Zaglic and Safikhanloo epithermal gold prospects, NW Iran. Geological Society of London, Special Publications 350: 133–147.

Gunow AJ, Ludington S Munoz JL (1980). Fluorine in micas from the Henderson molybdenite deposits, Colorado. Econ Geol 75: 1127–1137.

Hanley JJ, MacKenzie MK, Warren MR, Guillong M (2010). Distribution and origin of platinum-group elements in alkalic porphyry Cu–Au and low sulfidation epithermal Au deposits in the Canadian Cordillera. In: 11th International Platinum Symposium, 21–24 June, Sudbury, Canada.

Hasanpour S (2010). Metallogeny of the base and precious metals in Arasbaran zone, northwest Iran. PhD, Shahid Beheshti University, Tehran, Iran (in Persian with English abstract).

Hassanzadeh J (1993). Metallogenic and tectonomagmatic events in the SE sector of the Cenozoic active continental margin of Iran (Shahre Babak area, Kerman Province). PhD, University of California, Los Angeles, USA.

Hawthorne FC (1981). Crystal chemistry of the amphiboles. Rev Mineral Geochem 9A: 1–102.

Hezarkhani A (2006). Petrology of the intrusive rocks within the Sungun porphyry copper deposit, Azerbaijan, Iran. J Asian Earth Sci 27: 326–340.

Holland T, Blundy J (1994). Non-ideal interactions in calcic amphiboles and their bearing on amphibole–plagioclase thermometry. Contrib Mineral Petrol 116: 433–447.

Idrus A, Kolb J, Meyer FM (2007). Chemical composition of rock-forming minerals in copper-gold-bearing tonalite porphyries at the Batu Hijau deposit, Sumbawa island, Indonesia: implications for crystallization conditions and fluorine-chlorine fugacity. Resour Geol 57: 102–113.

Imai A (2000). Genesis of the Mamut porphyry Cu deposit, Sabah, East Malaysia. Resour Geol 50: 1–23.

Jacobs DC, Parry WT (1979). Geochemistry of biotite in the Santa Rita porphyry copper deposit, New Mexico. Econ Geol 74: 860–887.

John DA (2010). Porphyry Copper Deposit Model. Scientific Investigations Report 2010, 5070-B. Reston, VA, USA: US Geological Survey.

Kazemi-Mehrnia A (2010). Characteristics of leached capping and evolution of supergene enrichment of Northwest Kerman belt copper-molybdenum porphyry deposits. PhD, University of Shahid Beheshti, Tehran, Iran (in Persian with English abstract).

Kouhestani H, Gaderi M, Zaw K, Meffre S, Emami MH (2011). Geological setting and timing of the Chah Zard breccias-hosted epithermal gold-silver deposit in the Tethyan belt of Iran. Miner Deposita 47: 425–440.

Kranidiotis P, MacLean WH (1987). Systematics of chlorite alteration at the Phelps Dodge massive sulfide deposit, Matagami, Quebec. Econ Geol 82: 1898–1911.

Li J, Li G, Qin K, Xiao B, Chen L, Zhao J (2011). Mineralogy and mineral chemistry of the Cretaceous Duolong gold-rich porphyry copper deposit in the Bangongco arc, northern Tibet. Resour Geol 62: 19–41.

Mason DR (1978). Compositional variation in ferromagnesian minerals from porphyry copper generating and barren intrusions of the Western Highlands, Papua New Guinea. Econ Geol 73: 878–890.

Mohammadzadeh Z (2009). Geology, alteration and copper mineralization in Chahfiruzeh area, Share-Babak, Kerman province. MsC, University of Shahid Beheshti, Tehran, Iran (in Persian with English abstract).

Munoz JL (1984). F–OH and Cl–OH exchange in mica with application to hydrothermal ore deposits. Rev Mineral 13: 469–493.

Munoz JL (1992). Calculation of HF and HCl fugacities from biotite compositions: revised equations. Geological Society of America, Abstract Programs 24: A221.

NICICO (2008). Final Report of Exploration in the Chahfiruzeh Deposit. Internal Report. Tehran, Iran: National Iranian Copper Industries Co. (in Persian).

Pasava J, Vymazalova A, Kosler J, Koneev R, Jukov AV, Khalmatov RA (2010). Platinum-group elements in ores from the Kalmakyr porphyry Cu–Au–Mo deposit, Uzbekistan: bulk geochemical and laser ablation ICP-MS data. Miner Deposita 45: 411–418.

Reich M, Deditius A, Chryssoulis S, Lei JW, Ma CQ, Parada MA, Barra F, Mittermayr F (2013). Pyrite as a record of hydrothermal fluid evolution in a porphyry copper system: A SIMS/EMPA trace element study. Geochim Cosmochim Ac 104: 42–62.

Richards JP, Kerrich R (2007). Adakite-like rocks: their diverse origins and questionable role in metallogenesis. Econ Geol 102: 537–576.

Richards JP, Spell T, Rameh E, Razique A, Fletcher T (2012). High Sr/Y magmas reflect arc maturity, high magmatic water content, and porphyry Cu±Mo±Au potential: Examples from the Tethyan arcs of central and eastern Iran and western Pakistan. Econ Geol 107: 295–332.

Richards JP, Wilkinson D, Ullrich T (2006). Geology of the Sari Gunay epithermal gold deposit, northwest Iran. Econ Geol 101: 1455–1496.

Selby D, Nesbitt BE (2000). Chemical composition of biotite from the Casino porphyry Cu-Au-Mo mineralisation, Yukon, Canada: Evaluation of magmatic and hydrothermal fluid chemistry. Chem Geol 171: 77–93.

Shafiei B, Haschke M, Shahabpour J (2009). Recycling of orogenic arc crust triggers porphyry Cu-mineralization in Kerman Cenozoic arc rocks, southeastern Iran. Miner Deposita 44: 265–283.

Shafiei B, Shahabpour J (2012). Geochemical aspects of molybdenum and precious metals distribution in the Sarcheshmeh porphyry copper deposit, Iran. Miner Deposita 47: 535–543.

Siahcheshm K, Calagari AA, Abedini A, Lentz DR (2012). Halogen signatures of biotites from the Maher-Abad porphyry copper deposit, Iran: characterization of volatiles in syn- to post-magmatic hydrothermal fluids. Int Geol Rev 54: 1353–1368.

Stöcklin J (1968). Structural history and tectonics of Iran: a review. Am Assoc Petrol Geol Bull 52: 1229–1258.

Taghipour N, Aftabi A, Mathur R (2008). Geology and Re–Os geochronology of mineralization of the Miduk porphyry copper deposit, Iran. Resour Geol 58: 143–160.

Verdel C, Wernicke BP, Hassanzadeh J, Guest B (2011). A Paleogene extensional arc flare-up in Iran. Tectonics 30: 19.

Waterman GC, Hamilton RL (1975). The Sar Cheshmeh porphyry copper deposit. Econ Geol 70: 568–576.

Whitney DL, Evans BW (2010). Abbreviations for names of rock-forming minerals. Am Mineral 95: 185–187.

Xianwu B, Ruizhong H, Hanley JJ, Mungall JE, Jiantang P, Linbo S, Kaixing W, Yan S, Hongli L, Xiaoyan H (2009). Crystallisation conditions (T, P, fO_2) from mineral chemistry of Cu- and Au-mineralized alkaline intrusions in the Red River-Jinshajing alkaline igneous belt, western Yunnan province, China. Miner Petrol 96: 43–58.

Zarasvandi A, Liaghat S, Zentilli M (2005). Geology of the Darreh-Zerreshk and Ali-Abad porphyry copper deposits, central Iran. Int Geol Rev 47: 620–646.

Zhu C, Sverjensky DA (1992). Partitioning of F-Cl-OH between biotite and apatite. Geochim Cosmochim Ac 56: 3435–3467.

Appendix 1. Chemical composition of the sericite of phyllic alteration from the Chahfiruzeh porphyry.

(Sample: CHF06-413-Chahfiruzeh porphyry.)

	an1	an2	an4	an6	an8	an9	an11	an13	an14	an15	an16	an18	an20	an22	an23	an25	an27	an28	an29	an31	an33	an35	an36	an37	an38
SiO_2	41.876	43.533	42.292	42.681	44.252	43.092	43.254	42.972	45.247	42.425	45.742	43.6	45.733	42.768	42.459	42.363	41.943	43.097	42.609	43.586	41.91	43.932	42.555	42.7	42.623
TiO_2	0.325	0.119	0.272	0.022	0.315	0.354	0.126	0.108	0	0.052	0.099	0.455	0.194	0.468	0.45	0	0.42	0	0.095	0.036	0.249	0.163	0.096	0.119	0.08
Al_2O_3	28.756	30.199	29.217	30.355	28.694	29.235	29.546	28.73	30.901	30.09	29.633	29.874	28.375	30.076	28.992	29.559	29.746	29.717	30.006	28.281	29.466	30.894	28.731	29.499	28.961
FeO	5.468	3.63	4.996	3.812	4.406	4.712	3.948	4.4	3.56	4.571	2.985	4.409	3.896	4.449	4.323	4.351	4.304	4.23	4.587	4.718	4.919	4.285	5.01	4.193	4.901
MnO	0.076	0.06	0.053	0.072	0.019	0	0.001	0	0	0.041	0.068	0.039	0.054	0.036	0.013	0.045	0.016	0	0	0.04	0.017	0	0	0.01	0
MgO	4.138	2.875	4.355	2.254	3.559	3.108	2.629	4.269	2.004	2.828	2.133	3.736	1.869	3.017	3.131	3.547	3.277	3.393	3.732	4.127	4.109	1.964	4.204	3.675	4.056
CaO	0.008	0.037	0.013	0.013	0	0.038	0	0.027	0.05	0.004	0.067	0.006	0	0.001	0.041	0.012	0.006	0.011	0.01	0.049	0	0	0.659	0.045	0.009
Na_2O	0.143	0.247	0.21	0.467	0.252	0.477	0.448	0.354	0.439	0.426	0.187	0.431	0.125	0.402	0.311	0.323	0.239	0.331	0.441	0.405	0.352	0.446	0.318	0.385	0.438
K_2O	9.282	8.994	9.465	8.232	8.901	8.56	11.012	9.357	8.647	8.341	8.158	8.572	7.755	8.304	11.811	9.348	8.968	8.941	10.945	11.354	8.982	8.6	8.9	8.735	8.545
F	0.24	0.506	0	0.6	0.336	0.335	0	0	0	0	0.098	0	0.578	0	0	0.666	0.264	0.666	0.097	0.693	0.214	0	0.382	0	0
Cl	0.006	0.001	0.003	0.003	0.006	0.008	0.006	0.009	0	0.003	0	0.006	0.002	0.003	0.008	0.007	0.006	0.006	0.009	0.005	0.012	0.005	0.006	0.005	0.008
Total	90.216	89.988	90.875	88.257	90.598	89.776	90.969	90.224	90.848	88.78	89.129	91.127	88.338	89.523	91.537	89.939	89.077	90.111	92.488	93.001	90.137	90.288	90.699	89.365	89.619

Appendix 2.1. Chemical composition of chlorite from propylitic alteration of post-ore diorite.

CHF30-550.40 (Diorite)								
	an14	an15	an16	an19	an22	an23	an35	an55
SiO_2	26.317	26.458	27.683	26.911	26.906	28.647	26.536	27.724
TiO_2	0.005	0.012	0	0.016	0.056	0	0	0
Al_2O_3	19.039	18.194	18.455	18.396	18.813	17.668	18.275	18.491
FeO	21.718	21.32	21.466	21.769	22.887	21.566	23.309	21.943
MnO	0.436	1.041	0.299	1.271	0.445	0.313	0.442	0.318
MgO	17.958	18.059	18.185	17.16	16.893	18.237	16.927	18.334
CaO	0.032	0.01	0.058	0.023	0.048	0.084	0.04	0.055
Na_2O	0	0	0.033	0	0.025	0.027	0.012	0.002
K_2O	0.024	0	0.013	0.015	0.03	0.016	0.017	0
F	0.243	0.164	0.224	0	0.142	0	0.391	0
Cl	0.004	0	0.001	0	0	0	0.002	0.001
H2O (calc.)	10.65	10.61	10.8	10.73	10.72	10.97	10.49	10.97
Total	96.43	95.87	97.22	96.29	96.97	97.53	96.44	97.84
	Calculation on the basis of 14 oxygens							
Si	2.199	2.226	2.282	2.255	2.243	2.349	2.236	2.273
Al^{IV}	1.801	1.774	1.718	1.745	1.757	1.651	1.764	1.727
Sum_T	4	4	4	4	4	4	4	4
Al^{VI}	0.072	0.029	0.074	0.07	0.09	0.055	0.049	0.058
Ti	0	0.001	0	0.001	0.004	0	0	0
Fe2	1.517	1.5	1.48	1.526	1.596	1.479	1.642	1.505
Mn	0.031	0.074	0.021	0.09	0.031	0.022	0.032	0.022
Mg	2.237	2.265	2.235	2.144	2.099	2.229	2.126	2.241
Ca	0.003	0.001	0.005	0.002	0.004	0.007	0.004	0.005
Na	0	0	0.005	0	0.004	0.004	0.002	0
K	0.003	0	0.001	0.002	0.003	0.002	0.002	0
Sum cations	7.863	7.87	7.821	7.835	7.831	7.798	7.857	7.831
F	0.128	0.087	0.117	0	0.075	0	0.208	0
Cl	0.001	0	0	0	0	0	0.001	0
X_{Fe}	0.4	0.4	0.4	0.42	0.43	0.4	0.44	0.4
X_{Mg}	0.6	0.6	0.6	0.58	0.57	0.6	0.56	0.6
T °C	238.59	235.72	229.79	234.13	236.15	222.69	237.63	230.74

Appendix 2.2. Chemical composition of chlorite in Chahfiruzeh porphyry from the phyllic alteration zone.

	CHF06-413 (Chahfiruzeh porphyry)						
	an17	an21	an24	an3	an34	an5	an7
SiO_2	25.856	25.504	25.64	25.856	26.79	25.561	26.643
TiO_2	0.02	0.08	0.115	0.039	0.087	0.054	0.073
Al_2O_3	19.771	19.589	18.239	20.797	21.119	19.729	19.629
FeO	21.073	21.907	20.89	19.754	19.27	22.06	20.148
MnO	0.346	0.309	0.466	0.138	0.176	0.369	0.371
MgO	18.6	18.514	16.33	20.267	20.384	18.034	19.022
CaO	0.027	0.011	0.044	0.001	0.061	0.016	0
Na_2O	0.045	0	0.012	0.001	0.024	0.074	0
K_2O	0.058	0.003	0.012	0	0.001	0.006	0
F	0.04	0.02	0	0	0.101	0	0.16
Cl	0.001	0.001	0.002	0	0.002	0.002	0.002
H2O (calc.)	10.81	10.78	10.3	11.07	11.22	10.78	10.85
Total	96.65	96.72	92.05	97.92	99.24	96.68	96.9
	Calculation on the basis of 14 oxygens						
Si	2.147	2.126	2.239	2.101	2.139	2.133	2.193
Al^{IV}	1.853	1.874	1.761	1.899	1.861	1.867	1.807
Sum_T	4	4	4	4	4	4	4
Al^{VI}	0.081	0.049	0.114	0.091	0.124	0.072	0.096
Ti	0.001	0.005	0.008	0.002	0.005	0.003	0.005
Fe2	1.464	1.527	1.525	1.342	1.286	1.539	1.387
Mn	0.024	0.022	0.034	0.009	0.012	0.026	0.026
Mg	2.303	2.301	2.126	2.455	2.426	2.243	2.334
Ca	0.002	0.001	0.004	0	0.005	0.001	0
Na	0.007	0	0.002	0	0.004	0.012	0
K	0.006	0	0.001	0	0	0.001	0
Sum cations	7.888	7.905	7.814	7.899	7.862	7.897	7.848
F	0.021	0.011	0	0	0.051	0	0.083
Cl	0	0	0.001	0	0.001	0.001	0.001
X_{Fe}	0.39	0.4	0.42	0.35	0.35	0.41	0.37
X_{Mg}	0.61	0.6	0.58	0.65	0.65	0.59	0.63
T °C	243.36	246.32	235.83	245.26	241.24	246.32	237.00

Appendix 2.3. Chemical composition of chlorite from potassic zones in Chahfiruzeh porphyry and andesite.

CHF31-578.30 (Chahfiruzeh porphyry)																	CHF35-416.50 (Andesite)			
	an14	an15	an20	an22	an23	an34	an39	an46	an58	an62	an71	an72	an74	an8	an80	an84	an10	an11	an2	an3
SiO_2	27.055	28.648	27.791	28.638	27.71	27.617	28.596	28.937	28.528	29.177	26.909	27.1	27.514	27.276	27.776	27.534	27.586	27.128	26.315	26.197
TiO_2	0.087	0.284	0.073	0	0.07	0.084	0.091	0	0.081	0.079	0.057	0.06	0.079	0.071	0	0.084	0.179	0.084	0.283	0.135
Al_2O_3	16.62	16.301	17.66	16.864	16.77	18.283	17.41	16.359	17.179	16.786	18.905	19.834	18.114	18.782	17.421	17.421	22.252	22.252	20.858	20.131
FeO	21.854	18.6	21.375	20.158	21.874	19.995	20.472	20.345	19.867	20.191	20.363	19.596	20.708	20.813	22.606	19.988	16.551	17.973	19.786	17.74
MnO	0.163	0.15	0.134	0.163	0.207	0.237	0.212	0.127	0.196	0.172	0.183	0.218	0.131	0.212	0.207	0.188	0.192	0.099	0.073	0.151
MgO	18.716	20.025	19.086	19.836	18.943	20.196	19.687	19.976	20.14	20.475	19.936	19.139	19.693	21.229	18.472	20.483	18.966	20.762	19.855	20.486
CaO	0.045	0.18	0.032	0.002	0.046	0.048	0.049	0.09	0.051	0.041	0	0.066	0.034	0.041	0.027	0.035	0.065	0.101	0.074	0.083
Na_2O	0.022	0.049	0.05	0.025	0.029	0.031	0.023	0.026	0	0	0.034	0.021	0	0.033	0.052	0	0.038	0	0.008	0.002
K_2O	0.006	0.131	0.003	0.034	0.005	0.012	0.094	0.017	0	0.007	0.027	0.007	0	0.004	0.006	0.02	0.021	0.01	0.017	0
F	0	0.18	0.163	0	0.684	0.144	0	0.227	0	0	0.326	0.554	0	0.605	0	0	0	0.467	0	0.02
Cl	0.001	0.002	0	0	0	0	0.001	0	0.002	0	0	0.001	0	0.002	0	0.002	0.002	0.003	0	0
H2O (calc.)	10.63	10.74	10.84	10.93	10.47	10.96	11.03	10.84	10.99	11.1	10.83	10.74	10.96	10.93	10.88	10.91	11.22	11.22	11.14	10.93
Total	95.2	95.29	97.21	96.65	96.81	97.61	97.67	96.94	97.03	98.03	97.57	97.34	97.23	100	97.45	96.66	97.07	100.1	98.41	95.88
	Calculation on the basis of14 oxygens								Calculation on the basis of14 oxygens								Calculation on the basis of 14 oxygens			
Si	2.289	2.38	2.291	2.356	2.31	2.253	2.332	2.378	2.335	2.364	2.204	2.215	2.259	2.187	2.296	2.269	2.212	2.133	2.125	2.154
Al^{IV}	1.656	1.595	1.709	1.634	1.646	1.747	1.668	1.583	1.656	1.602	1.796	1.785	1.741	1.774	1.696	1.691	1.788	1.867	1.875	1.846
Sum_T	3.945	3.975	4	3.99	3.956	4	4	3.961	3.991	3.966	4	4	4	3.961	3.992	3.96	4	4	4	4
Al^{VI}	0	0	0.005	0	0	0.01	0.004	0	0	0	0.028	0.124	0.01	0	0	0	0.313	0.193	0.108	0.103
Ti	0.006	0.018	0.005	0	0.004	0.005	0.006	0	0.005	0.005	0.004	0.004	0.005	0.004	0	0.005	0.011	0.005	0.017	0.008
Fe2	1.546	1.292	1.474	1.387	1.525	1.364	1.396	1.398	1.36	1.368	1.395	1.34	1.422	1.396	1.563	1.378	1.11	1.182	1.336	1.22
Mn	0.012	0.011	0.009	0.011	0.015	0.016	0.015	0.009	0.014	0.012	0.013	0.015	0.009	0.014	0.014	0.013	0.013	0.007	0.005	0.011
Mg	2.361	2.48	2.345	2.433	2.354	2.457	2.393	2.448	2.457	2.473	2.434	2.332	2.41	2.538	2.277	2.517	2.267	2.433	2.39	2.511
Ca	0.004	0.016	0.003	0	0.004	0.004	0.004	0.008	0.004	0.004	0	0.006	0.003	0.004	0.002	0.003	0.006	0.009	0.006	0.007
Na	0.004	0.008	0.008	0.004	0.005	0.005	0.004	0.004	0	0	0.005	0.003	0	0.005	0.008	0	0.006	0	0.001	0
K	0.001	0.014	0	0.004	0.001	0.001	0.01	0.002	0	0.001	0.003	0.001	0	0	0.001	0.002	0.002	0.001	0.002	0
Sum cations	7.879	7.814	7.849	7.829	7.864	7.862	7.832	7.83	7.831	7.829	7.882	7.825	7.859	7.922	7.857	7.878	7.728	7.83	7.865	7.86
F	0	0.095	0.085	0	0.361	0.074	0	0.118	0	0	0.169	0.286	0	0.307	0	0	0	0.232	0	0.01
Cl	0	0.001	0	0	0	0	0	0	0.001	0	0	0	0	0.001	0	0.001	0.001	0.001	0	0
X_{Fe}	0.4	0.34	0.39	0.36	0.39	0.36	0.37	0.36	0.36	0.36	0.36	0.36	0.37	0.35	0.41	0.35	0.33	0.33	0.36	0.33
X_{Mg}	0.6	0.66	0.61	0.64	0.61	0.64	0.63	0.64	0.64	0.64	0.64	0.64	0.63	0.65	0.59	0.65	0.67	0.67	0.64	0.67
T °C	223.22	212.30	228.09	217.92	221.41	229.89	222.26	212.51	220.25	214.52	235.09	233.92	230.00	232.01	228.20	223.22	232.01	240.39	243.46	238.16